

PAPER

Spectroscopic investigation on the near-substrate plasma characteristics of chromium HiPIMS in low density discharge mode

To cite this article: Xiao Zuo *et al* 2020 *Plasma Sources Sci. Technol.* **29** 015013

View the [article online](#) for updates and enhancements.



IOP | ebooks™

Bringing you innovative digital publishing with leading voices to create your essential collection of books in STEM research.

Start exploring the collection - download the first chapter of every title for free.

Spectroscopic investigation on the near-substrate plasma characteristics of chromium HiPIMS in low density discharge mode

Xiao Zuo^{1,2,3,5} , Dong Zhang^{1,2,3,5}, Rende Chen^{1,2}, Pelling Ke^{1,2,3,6}, Magnus Odén⁴ and Aiyang Wang^{1,2,3,6} 

¹Key Laboratory of Marine Materials and Related Technologies, Zhejiang Key Laboratory of Marine Materials and Protective Technologies, Ningbo Institute of Materials Technology and Engineering, Chinese Academy of Sciences, Ningbo, 315201, People's Republic of China

²Ningbo Institute of Industrial Technology, Chinese Academy of Sciences, Ningbo, 315201, People's Republic of China

³The Center of Materials Science and Optoelectronics Engineering, University of Chinese Academy of Sciences, Beijing, 100049, People's Republic of China

⁴Department of Physics, Chemistry, and Biology, Linköping University, Linköping SE-58183, Sweden

E-mail: kepl@nimte.ac.cn and aywang@nimte.ac.cn

Received 16 August 2019, revised 16 November 2019

Accepted for publication 26 November 2019

Published 28 January 2020



CrossMark

Abstract

High power impulse magnetron sputtering (HiPIMS) discharge promises high ionization fraction and energetic ions in comparison with dc magnetron sputtering discharge. But acknowledge on the characteristics of HiPIMS plasma in the near-substrate region (substrate vicinity), which is of great importance for film deposition, is still limited. Here, optical emission spectroscopy (OES) combined with the collisional-radiative modelling are developed and used to determine the electron temperature and the number density of neutral sputtered atom for the chromium HiPIMS plasma in substrate vicinity. The OES analysis demonstrated the HiPIMS discharge of Cr sputtering process in low density mode was dominated by the electron impact ionization of argon atoms and excitation of chromium atoms. As the HiPIMS plasma in the substrate vicinity is far from the local thermal equilibrium state, the relative intensities of transition lines to ArI $4p$ states was used to calculate the electron temperature. Subsequently, the neutral chromium atoms density about 10^{17} m^{-3} was reported in the near-substrate region. Our findings have important implications for species generation in low density HiPIMS discharge, with applications in synthesis of dense chromium coatings.

Keywords: high power impulse magnetron sputtering, optical emission spectroscopy, electron excitation temperature, chromium atoms density, near-substrate region

1. Introduction

High power impulse magnetron sputtering (HiPIMS) is a novel technique for ionized physical vapor deposition [1, 2]. Of special interest are high density plasmas which exhibit a high ionization fraction of metal atoms [3–5], because it can lead to dense and

uniform film structures [6–8]. Emerging applications of HiPIMS are as sources for metal ion beams [9–11], and a platform in the synthesis of high-conductive metal thin films [12] or dense anti-oxidation coatings [8, 13]. Significant efforts are being made to develop HiPIMS processes designed for oxidation resistance coatings, which could be a strategy to improve the safety of accident-tolerant fuels for the light water reactors [14, 15].

Together with its promising technological and industrial use, HiPIMS discharge has also been the subject of significant

⁵ Xiao Zuo and Dong Zhang contributed to this work equally.

⁶ Authors to whom any correspondence should be addressed.

academic interest [16–19], in particular by the plasma source science and technology community. The high degree of controlling parameters exhibited by HiPIMS results in distinct operation modes [20]. This flexibility is also responsible for the large degree of microstructural variability in the deposited coatings. Anders reported that the runaway to a high density discharge is based on self-sputter in conjunction with the recycling of gas atoms in the magnetic field affected pre-sheath [21]. Therefore, the threshold to the high density HiPIMS discharge has been identified with the onset of sustained self-sputter. However, the sustained self-sputter process can only operate when the power density is very high (typically several 100 W cm^{-2} [22]) [23], which is still a great challenge for low melting point targets and large scale industrial applications. Additionally, HiPIMS discharge with chromium target is hard to enter high density discharge mode. Thus, here we focus our research on the low density HiPIMS discharge with intermediate target dimensions. First investigations of sputtering from Cr targets with optical emission spectroscopy (OES) have shown a significant enhancement of ion/atom ratio by HiPIMS compared with conventional dc magnetron sputtering [24–26]. To clarify the mechanisms involved in HiPIMS plasma formation such as energy coupling, electron heating, chemical reactions with neutral background gas, and particle transportation in non-reactive and reactive mode, diversified diagnostic techniques such as Langmuir probe, OES, optical absorption spectroscopy, laser induced fluorescence, laser Thomson scattering are mainly used to track the ground-state, metastable, and charged species in the ionization region near the cathodic target [27–29]. Very few of them discuss the reaction paths of excited states in the near-substrate region. However, many factors in the HiPIMS deposition are still not well understood. Therefore, the understanding of these processes emerge as the key for the efficient optimization of HiPIMS deposition processes with the goal of structural control on coating materials for possible applications. Here we explore the parameters of HiPIMS plasma in the near-substrate region using OES in order to understand more fully the role and creation mechanism of the various species.

This paper deals with the near-substrate plasma characteristics of chromium HiPIMS in low density discharge mode by absolute calibrated OES. With the experimental setup shown here it is possible to determine parameters such as electron temperature by the modified Boltzmann method, and neutral particle densities by the OES model.

2. Experimental setup

The experimental setup is schematized in figure 1. The magnetron cathode is a high purity chromium target (Advanced Technology & Materials Co., Ltd) with the dimensions of $400 \text{ mm} \times 100 \text{ mm} \times 7 \text{ mm}$. The maximum magnetic induction intensity is $\sim 260 \text{ G}$. The magnetron (Vacpro Advanced Coating Process Co., Ltd) is located inside a $\Phi 600 \text{ mm} \times 600 \text{ mm}$ stainless steel chamber, in which it is surrounded by a guard ring and by the chamber wall at

ground potential. A cuboid substrate holder ($400 \text{ mm} \times 100 \text{ mm} \times 100 \text{ mm}$) is installed facing toward the target with a surface distance of 12 cm .

After an ultimate vacuum of about 1.2×10^{-5} Torr, Ar was introduced into the chamber. The target surface was cleaned by dc magnetron sputtering. A high power pulse unit (HPPMS-20 k, PTL) operating in unipolar mode was used to power the target at constant peak voltage mode. Thus, the pulse voltage in this paper refers to the peak voltage. The target voltage and current were monitored using a combined current transducer (LEM LT58-S7) and a voltage probe (UT-V23, UNI-T). The data were recorded with a digital storage oscilloscope (Tektronix TDS 1012C-SC). The electrical setup is described detail in [30]. The average discharge current (I_a) was calculated by

$$I_a = \frac{1}{T} \int_0^T I_t(t) dt, \quad (1)$$

where, T and I_t are the pulse period and the transient target current, respectively. The current density and power density were calculated by the current and power over the surface of the target covered by the plasma, which was introduced by Wendt [31]. The calculation of this effective surface in our case can be found in a previous publication [30].

OES spectra were acquired via the optical fiber and analyzed by a spectrometer (Acton SP2500, Princeton Instruments) equipped with a grating of 1200 g mm^{-1} and $10 \mu\text{m}$ wide slit. This spectrometer was calibrated by typical mercury pen lamps. The collimated optical fiber port was installed parallel to the magnetron surface with a distance of $\sim 10 \text{ cm}$ (as shown in figure 1). The collimator could exclude the light with the incident angle deviated more than 5° from normal direction. To avoid the films coated on the lens, an aluminum tube with the inner dimension of $\varnothing 3 \text{ mm} \times 90 \text{ mm}$ was installed before the collimator. This made the deviation angle reduced to $\sim 2^\circ$, which could only promise emission light from a taper region with the base length less than $\sim 2 \text{ cm}$ entering the collimator. In addition the chamber walls were sheltered by liner plates to avoid coatings, which enhanced the diffusion by the walls. Therefore, the emission light from the target vicinity was able to be excluded in the largest extension. The integral time and high voltage was set as 1000 ms and 815 V , respectively. When the Single Point Scan mode was selected, typical atomic spectrum lines of Ar and Cr were observed. In order to reduce errors in the plasma parameters, several independent experiments were performed under the same conditions and the results represented the average of five independent experiments.

A single Langmuir probe (LP-500 ALP system, Impedans Ltd) was applied to measure the electron density and electron temperature in the same plasma region at substrate vicinity. The size of the tungsten tip is $\varnothing 0.35 \text{ mm} \times 8.5 \text{ mm}$. The distance from the probe tip to the target surface is around 10 cm . During the tests, the time integral mode was applied.

Here, we controlled three main parameters (like pressure, pulse voltage, and discharge power) to investigate the HiPIMS plasma generated under different conditions. The working gas was Ar with an adjustable flow rate up to

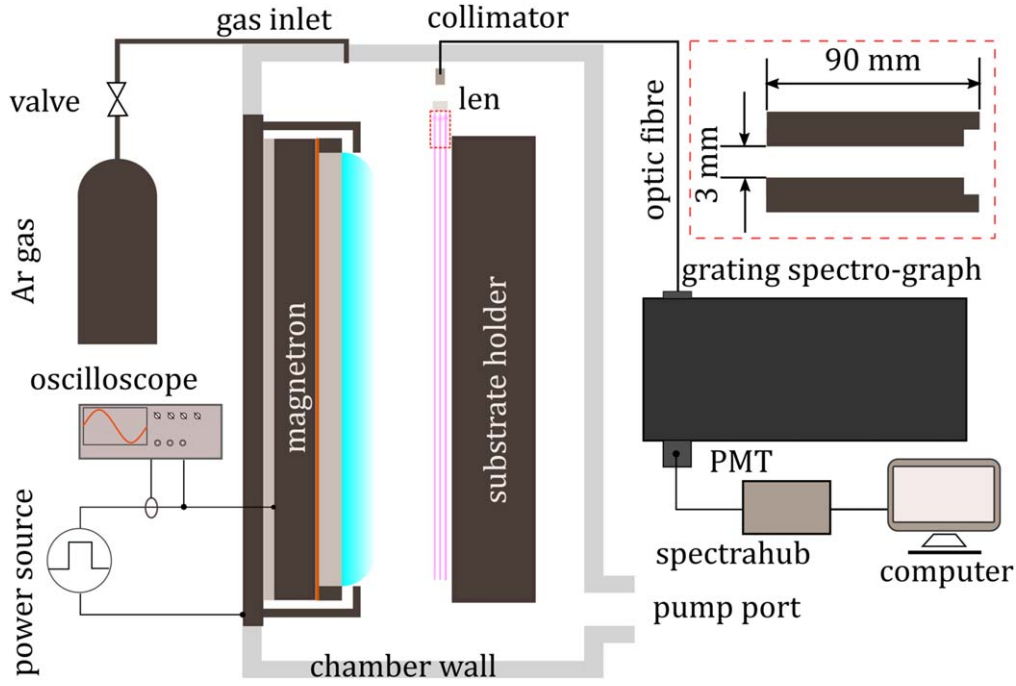


Figure 1. A schematic graph on the setup of the HiPIMS with the arrangement for discharge voltage/current waveforms measurement and optical emission spectroscopy. The red dash region demonstrates the dimensions of an aluminum tube installed before the collimator.

100 sccm by a calibrated mass flow controller. The working pressure was controlled by a variable gate valve (VAT Group AG). The parameters for these different conditions are list in the table 1.

3. Determination of the neutral chromium density and the electron temperature

3.1. OES model

From the kinetic modelling of the measured excited Cr and Ar atoms spectral line intensities, we can deduce the Cr atoms density in the HiPIMS discharge [32]. Assuming direct electronic excitation process from ground state, uniform plasma emission and no re-absorption, the signal intensity detected corresponding to the transition $m \rightarrow n$, can be written as [33]

$$I_{mn} = [X_m^*] R_{mn} h \nu_{mn} A_{mn} d\Omega', \quad (2)$$

where R_{mn} is the spectral response, ν_{mn} is the frequency of the emission light, A_{mn} is the transition probability, $[X_m^*]$ is the Ar or Cr atoms number density in the excited state 'm', and $d\Omega'$ is the constant solid angle for each discharge condition. Further assuming the excited state X_m^* decays by radiative process, its number density is given by

$$[X_m^*] = [X_m] n_e \tau_k K_{exc}^e \quad (3)$$

$[X_m]$ is the density of Ar or Cr atoms number density in the ground state, τ_k is the radiation lifetime, n_e is the electron density, and K_{exc}^e is the electron excitation rate. Considering two transitions $m \rightarrow n$ and $k \rightarrow l$ for chromium and argon

atoms, respectively, their line intensity ratio is obtained

$$\frac{I_{mn}^{Cr}}{I_{kl}^{Ar}} = \frac{[Cr^*] R_{mn}^{Cr} \nu_{mn}^{Cr} A_{mn}^{Cr}}{[Ar^*] R_{kl}^{Ar} \nu_{kl}^{Ar} A_{kl}^{Ar}}. \quad (4)$$

Thus, the number density of ground-state chromium atom can be deduced from equations (3) and (4). From equation (3), we can write the excited state Ar density $[Ar_k^*]$ as

$$[Ar_k^*] = [Ar] n_e \tau_k C_{0k}^e \quad (5)$$

C_{0k}^e is the electron excitation coefficient $C_{0k}^e = \langle \nu \sigma_{0k} \rangle$ with σ_{0k} being the cross section for excitation from ground state to state k by electron impact. A relation similar to equation (5) can be written for Cr_m^* density

$$[Cr_m^*] = [Cr] n_e \tau_m C_{0m}^e. \quad (6)$$

The relation between Cr and Ar ground state densities can be deduced from equations (4)–(6)

$$\frac{[Cr]}{[Ar]} = \frac{I_{mn}^{Cr} R_{mn}^{Cr} \nu_{kl}^{Ar} C_{0k}^e \tau_k A_{kl}^{Ar}}{I_{kl}^{Ar} R_{kl}^{Ar} \nu_{mn}^{Cr} C_{0m}^e \tau_m A_{mn}^{Cr}}. \quad (7)$$

When the formation of the excited state is not simply direct, the electronic collision exchanges with other excited levels and radiative cascades from upper levels must be considered. Therefore, equation (5) can be rewritten as

$$[Ar_k^*] = [Ar] n_e \tau'_k C'_{0k} \quad (8)$$

C'_{0k} and τ'_k are defined by

$$[Ar] n_e C'_{0k} = n_e \left([Ar] C_{0k}^e + \sum_{l=k} [Ar_k^*] C_{lk}^e \right) + \sum_{l>k} [Ar_k^*] A_{lk} \quad (9)$$

in which the second term on the right-hand side represents

Table 1. Detailed parameters for the five different experimental groups.

Parameters					
Group	Working pressure (mTorr)	Pulse voltage (V)	Pulse width (μ s)	Pulse frequency (Hz)	Discharge power (kW)
A	0.5, 2.5, 5.0, 10.0, 20.0	600	\sim 200.0	50	Variable
B	2.5	400, 500, 600, 700, 800, 900, 950	\sim 200.0	50	Variable
C	2.5	Variable	Variable	Variable	1143, 1488, 1802, 2088, 2106, 2516, 2934, 3420, 3860

inelastic collisions from states m to state k and the third term for radiative cascades from upper levels, and

$$1/\tau'_k = \sum_{l < k} A_{kl} + n_e \sum_{l \neq k} C_{lk}^e + n_e C_k^e, \quad (10)$$

where C_k^e is the ionization rate of state k . Finally the relation (7) is replaced by:

$$\frac{[\text{Cr}]}{[\text{Ar}]} = \frac{I_{mn}^{\text{Cr}} R_{mn}^{\text{Cr}} v_{kl}^{\text{Ar}} C_{0k}^{\text{Cr}} \tau'_k A_{kl}^{\text{Ar}}}{I_{kl}^{\text{Ar}} R_{kl}^{\text{Ar}} v_{mn}^{\text{Cr}} C_{0m}^{\text{Cr}} \tau'_m A_{mn}^{\text{Cr}}}. \quad (11)$$

3.2. Determination of electron excitation temperature

Under the low density HiPIMS discharge conditions, deviations from local thermal equilibrium (LTE) occur. Due to the reduction of energy exchange by collisions, the electron temperature can be higher than that of heavy species. Only the higher energy levels can be in partial-LTE (p -LTE) and therefore represent the correct electron excitation temperature [34]. Thus, we use Ar neutral lines to calculate the excitation temperature. In order to determine the electron excitation temperature, the modified Boltzmann plot method is applied [35]. In the simplified corona balance model, the density of excited states as such is a very sensitive parameter as a function of the electron temperature. The state densities are balanced by two different processes: collisional excitation by electrons from the ground state and spontaneous emission of radiation. The modified Boltzmann formula is written as follows [36]

$$\ln \left(\frac{I_{kl} \lambda_{kl} \sum_{k>l} A_{kl}}{A_{kl} a_{0k}} \right) = -\frac{E_k}{k_B T_e} + \text{const} \quad (12)$$

in which a_{0k} is the coefficient in an exponential approximation of the electron-impact excitation rate coefficient from ground state to level k . Therefore, in this work we can obtain the chromium density and electron temperature for Cr HiPIMS in low density discharge mode.

4. Results

4.1. Spectroscopic measurements and the variation of emission intensity

The typical survey spectra for the near-substrate plasma in a range of 200–900 nm for chromium HiPIMS discharge are presented in figure 2. The emission spectra are dominated by excited Cr atoms, for instance, CrII and CrI in the UV–vis region, ArI in the IR region. These lines are identified by comparison to [37].

A summary of the emission lines chosen for the present study along with the relevant energy levels involved in the transitions is presented in table 2. The excitation energy of emitting levels from the ground state of Ar atom is above 11 eV, whereas the excitation energy for Cr is at around 3 eV [37]. Therefore, the emission of the argon lines depends on the presence of hot electrons, whereas the chromium

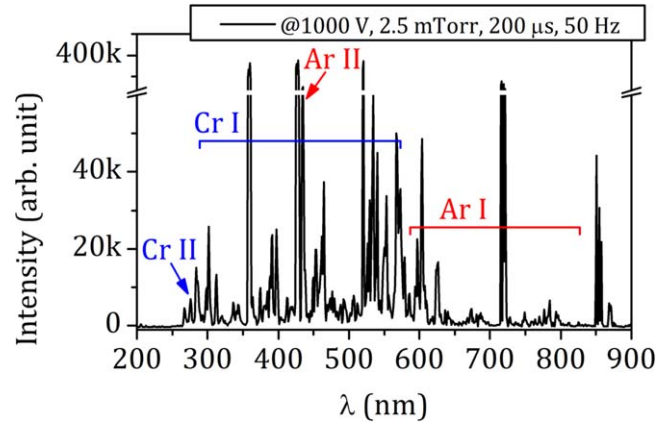


Figure 2. A typical emission spectrum of chromium HiPIMS plasma in the near-substrate region. λ is the transition wavelength.

emissions can also be excited by low-energy electrons. We also note that the Ar lines terminate in a lower state that is short-lived (radiative), whereas others terminate in long-lived (metastable) lower states. Being different from the condition in the ionization region where the Ar metastable has a relatively high density, also gives good insights into the ionization, excitation, gas rarefaction and refill processes [38–40], the Ar metastable show less distinct features in the substrate vicinity region as the density of Ar metastable becomes very low at the place outside the ionization region [39]. Therefore, we choose the Ar* radiative states to analyze the excitation process and calculate the excitation temperature and the Cr atom density in the topic of this work [41].

The number density of emitting atoms in our magnetron plasma is determined primarily by electron-driven processes such as electron impact excitation of the atom in its electronic ground state and by electron impact excitation of an excited metastable level that lies energetically below the emitting level. The rate of formation of excited species via electron-driven processes depends essentially on three parameters, the electron density (n_e) at a given electron energy, the electron temperature (T_e) and the density of the respective target species, N (ground-state or metastable atoms). The emitting levels can also be populated by radiative process via cascading from more higher-lying excited states that decay to the emitting level. Lastly, emitting levels can be populated collisionally by Penning excitation involving metastable atoms with sufficient energy. In the present case, this applies to Penning excitation of chromium by Ar metastable atoms. The efficiency of forming excited species via Penning excitation depends on the density of metastable atoms, which in turn is also determined by the rate of the electron-induced formation of metastable atoms from ground-state atoms.

The changes in some special emission line intensities with the variation of the average current (corresponding to the specific pulse voltage), the pressure and the discharge power of the HiPIMS discharge are investigated, as shown in figures 3–5. The emission intensity of lines of Cr⁺ (284.1 nm), Cr* (357.8, 359.5, 425.6, 427.6, 521.0 nm), Ar⁺ (434.9 nm), and Ar* (605.5, 750.6 nm) increases with the average current, indicating that when the pulse voltage rises,

Table 2. Spectroscopic data for emitted lines. λ is the wavelength of the transition (nm), the levels are given in general coupling notation apart for Ar I in Paschen notation, from upper (first) to lower, E_u is the energy of the upper level of the transition (eV), f is the oscillator strength (dimensionless) and A the spontaneous emission probability (s^{-1}). g_u is the Landé factor of the upper level.

Species	λ (nm)	A (s^{-1})	E_l (eV)	E_u (eV)	Low. level	Transition	g_u
Cr II	284.1	2.0e8	3.76	8.15	—	$3d^44p(z^4I^\circ) \rightarrow 3d^44a(a^4H)$	16
Cr I	335.3	1.2e5	0.00	3.69	Ground	$3d^44s4p(y^5P^\circ) \rightarrow 3d^54s(a^7S)$	7
	357.8	1.48e8	0.00	3.46		$3d^44s4p(y^7P^\circ) \rightarrow 3d^54s(a^7S)$	9
	359.5	1.5e8	0.00	3.44			7
	425.6	3.1e7	0.00	2.91		$3d^54p(z^7P^\circ) \rightarrow 3d^54s(a^7S)$	9
	427.6	3.0e7	0.00	2.89			7
	449.8	3.3e6	0.94	3.69	Metastable	$3d^44s4p(y^5P^\circ) \rightarrow 3d^54s(a^5S)$	7
	454.7	2.7e6	0.94	3.66			5
	494.4	1.9e5	0.94	3.44		$3d^44s4p(y^7P^\circ) \rightarrow 3d^54s(a^5S)$	7
	496.6	1.6e5	0.94	3.43			5
	505.3	5.4e4	0.94	3.39		$3d^44s4p(z^7D^\circ) \rightarrow 3d^54s(a^5S)$	5
507.4	1.5e5	0.94	3.38			3	
521.0	5.0e7	0.94	3.32		$3d^54p(z^5P^\circ) \rightarrow 3d^54s(a^5S)$	7	
Ar II	434.9	1.1e8	16.64	19.49	—	$3s^23p^44p \rightarrow 3s^23p^44s$	8
Ar I	583.6	5.2e5	13.17	15.29	Radiative	$3s^23p^55d \rightarrow 3s^23p^54p$	5
	605.5	1.4e6	13.09	15.14			7
	610.7	1.2e6	13.28	15.31			5
	720.9	2.4e6	13.30	15.02		$3s^23p^56s \rightarrow 3s^23p^54p$	3
	728.7	1.2e5	13.30	15.00		$3s^23p^54d \rightarrow 3s^23p^54p$	3
	770.7	6.3e4	13.17	14.78			7
	738.6	8.5e6	11.62	13.30		$3s^23p^54p(^2[3/2]) \rightarrow 3s^23p^54s(^2[3/2]^\circ)$	5
	750.6	4.0e7	11.62	13.27			1
	795.0	1.8e7	11.72	13.28	Metastable	$3s^23p^54p(^2[3/2]) \rightarrow 3s^23p^54s(^2[1/2]^\circ)$	3
	826.7	1.5e7	11.83	13.33			3
867.0	2.4e6	11.72	13.15			3	

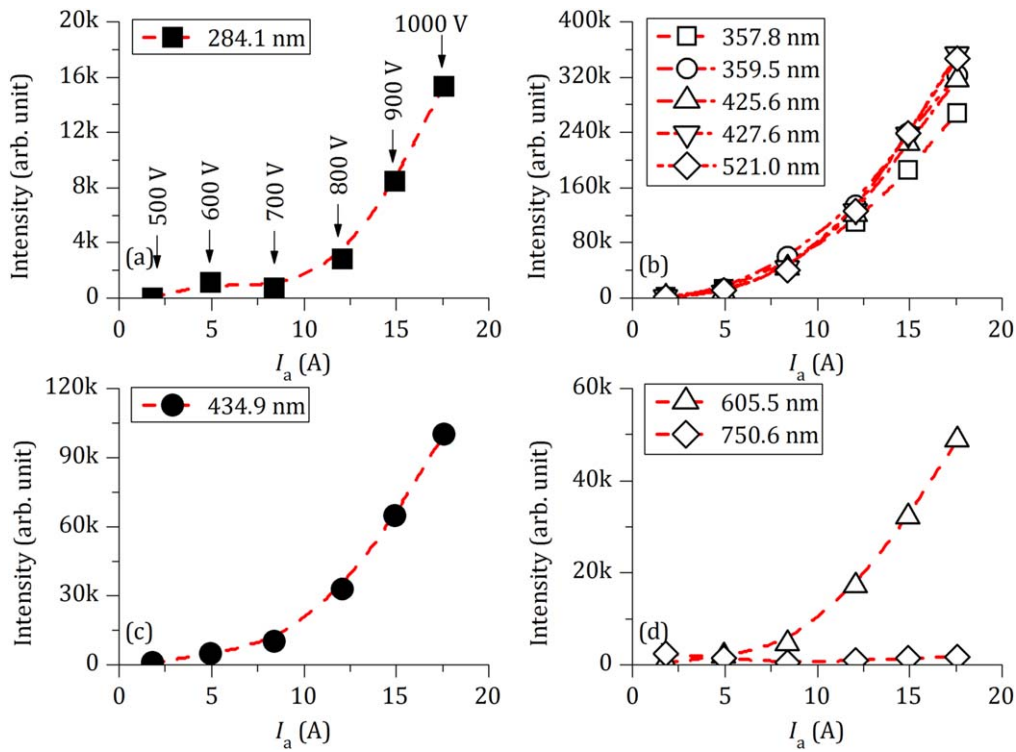


Figure 3. Emission intensities of the main lines in the substrate vicinity of chromium HiPIMS plasma as a function of the average target current (I_a) corresponding to the pulse voltage (U_p). The emission lines are Cr^+ (284.1 nm), Cr^* (357.8, 359.5, 425.6, 427.6, 521.0 nm), Ar^+ (434.9 nm), and Ar^* (605.5, 750.6 nm), respectively.

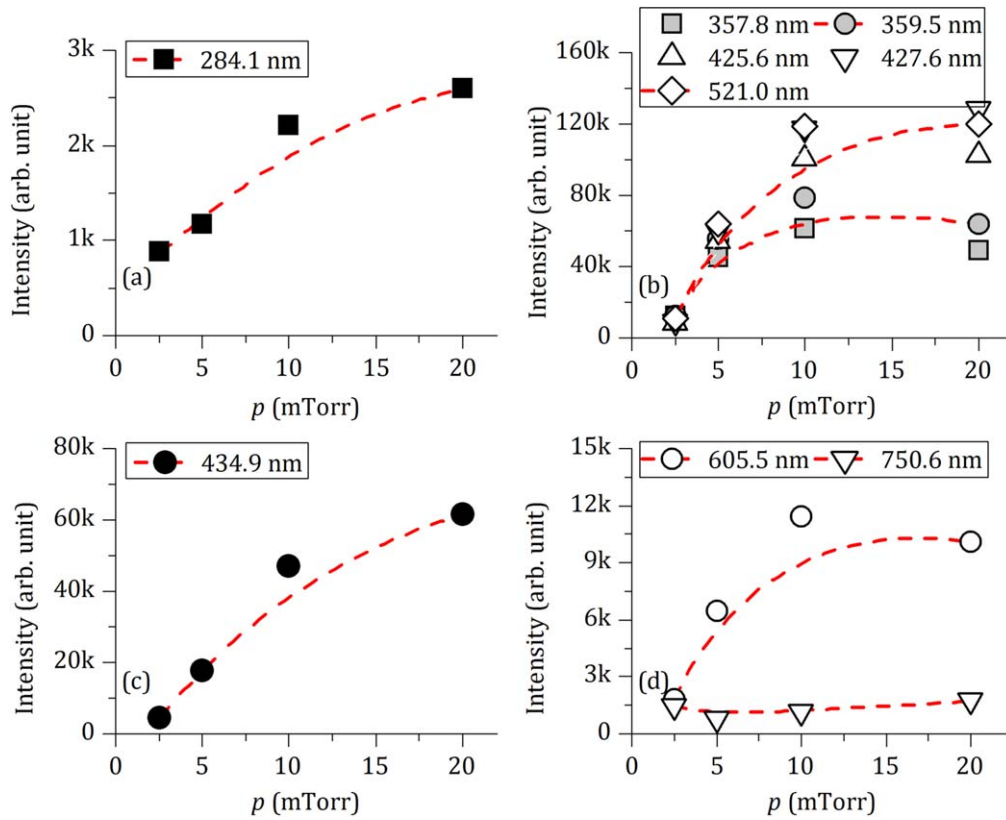


Figure 4. Emission intensities of the main lines in the near substrate region of chromium HiPIMS discharge as a function of working pressure (p). The emission lines are Cr⁺ (284.1 nm), Cr* (357.8, 359.5, 425.6, 427.6, 521.0 nm), Ar⁺ (434.9 nm), and Ar* (605.5, 750.6 nm), respectively.

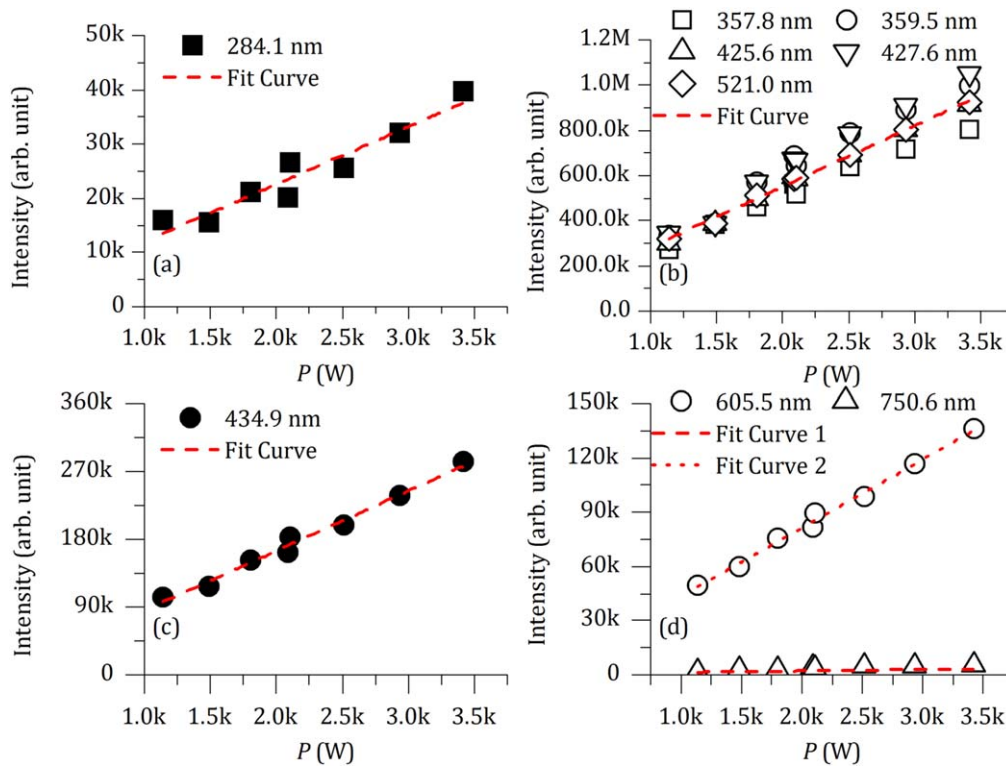


Figure 5. Emission intensities of the main lines in the near substrate region of the chromium HiPIMS discharge as a function of discharge power (P). The emission lines are Cr⁺ (284.1 nm), Cr* (357.8, 359.5, 425.6, 427.6, 521.0 nm), Ar⁺ (434.9 nm), and Ar* (605.5, 750.6 nm), respectively.

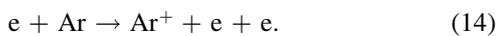
more Ar and Cr atoms are excited and ionized. Overall, the emission intensity of Cr^+ is much weaker than that of Cr^* for HiPIMS in the low density discharge mode. But the emission intensity of Ar^+ can compare with that of Ar^* , indicating a high ionization degree of Ar gas. As the sputter yield of Cr is above than 1.0 when the incident energy of Ar^+ is higher than 400 eV. Therefore, a large amount of sputtered out Cr atoms exist in HiPIMS plasma. As a result, a highest emission intensity of excited Cr atoms was observed. Although the increase of emission line intensities with pressure were also observed, its escalating rate became lower. The reason behind the difference between these two parameters is the variation of electron energy with the pulse voltage and working pressure. The improvement of pulse voltage led to direct increase of electron energy, however electron energy decreased with the increase of working pressure although the atom number density was increased.

The variation of emission intensity with discharge power was also investigated. As the nominal voltage was 1200 V, the discharge power with the increase pulse voltage at 2.5 mTorr was limited. Additionally, severe arcing happened when the pulse voltage was higher than 1000 V. Therefore, we adjusted the pulse frequency from 50 to 300 Hz, and the discharge power also increased from ~ 1.0 to ~ 3.5 kW, which means that the average power density increased to higher than ~ 0.01 kW cm^{-2} . As shown in figure 5, in the investigated discharge power range the emission intensities of excited and ionized atoms presented a linear increase tendency. Most of the intensity of emission lines increased with the discharge power except some Ar^* lines. From the slope of the fitting line, it can be found the emission intensity of Cr^* lines increased much faster than other lines especially the Cr^+ line. These results demonstrated that the collision processes of chromium HiPIMS plasma in low density mode was dominated by the ionization process of Ar atoms and excitation process of Cr atoms.

This can be understood by analyzing the mechanisms involved in the populating and depopulating processes. For the chromium species at the steady state, by equalizing the creation and losses terms [42]:

$$[\text{Cr}] = \frac{\gamma_{\text{Cr}} \times [\text{Ar}^+]}{\nu_{\text{wall}}^{\text{Cr}} + n_e k_{e,\text{Cr}}^{\text{products}}} \quad (13)$$

γ_{Cr} is the ionic collisions probability for Cr, $\nu_{\text{wall}}^{\text{Cr}}$ is the loss frequency of Cr by the diffusion process, $k_{e,\text{Cr}}^{\text{products}}$ is the rate coefficient. To investigate the behavior of [Cr], which depends on the argon ion density, we can follow the behavior of ionic emitted lines as functions of pulse voltage, pressure, and discharge power. The main creation mechanism for argon ions considered to be electronic collision, with the rate coefficient ($k_{e,\text{Ar}}^+$):



Further considering the following mechanisms for the creation of excited states of argon ions:

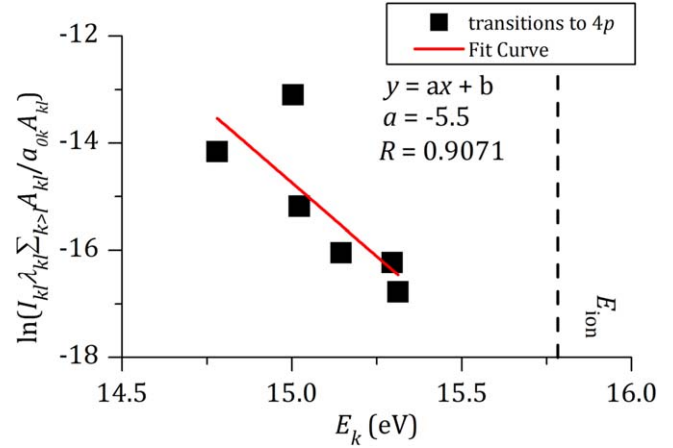
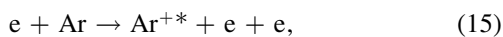
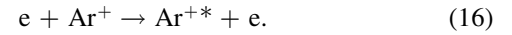


Figure 6. The modified Boltzmann plot for the Cr HiPIMS plasma in the near-substrate region, using emission lines measured for ArI 4p. The data indicate that the system of electrons and ArI are far from LTE, with a goodness of fit $R = 0.907$.



Then the excited argon ions density is expressed by [42]:

(a) argon ion excited from the argon neutral (see (15)):

$$I_{\text{Ar}^{+*}} = K^\nu \times n_e \times [\text{Ar}] \times C_{+*}^{\text{atom}} \quad (17)$$

(b) argon ion excited from the ion ground state (see (16)), if minor diffusion:

$$I_{\text{Ar}^{+*}} = K^\nu \times n_e \times [\text{Ar}] \times C_{+*}^{\text{ion}} \times C_+^{\text{coll}} \quad (18)$$

(c) argon ion excited from the ion ground state (see (16)), if dominant diffusion:

$$I_{\text{Ar}^{+*}} = K^\nu \times n_e \times [\text{Ar}] \times C_{+*}^{\text{ion}} \times n_e \times C_+^{\text{diff}}, \quad (19)$$

where K^ν is a constant specific to each emitted line which includes the detection system response, the $C_{\text{species}}^{\text{coll/diff}}$ constants are defined as the ratio between the creation coefficient and the loss coefficient with dimension of volume in the case of diffusion (C_+^{diff}) or dimensionless in the case of collisional losses (C_+^{coll}). Since the average current is proportional to the electron density. By fitting the scatter lines in figure 3 with the above equations (17)–(19), it can be easily found that the excited argon ions are mainly excited from the ion ground state, and its loss process in the near-substrate region is diffusion process dominated.

4.2. Electron excitation temperature measurements

The electron temperature is determined from emission line intensities using the modified Boltzmann plot method. Figure 6 shows a modified Boltzmann plot for the chromium HiPIMS plasma at 2.5 mTorr, 600 V, 200 μs and 50 Hz. The data indicate that the system of electrons and ArI are far from LTE, with a goodness of fit $R = 0.907$. Similar plots were obtained for all conditions examined. Linear regression was performed on all Boltzmann plots, giving the electron temperatures and the associated errors for all conditions. Results are shown in figure 7.

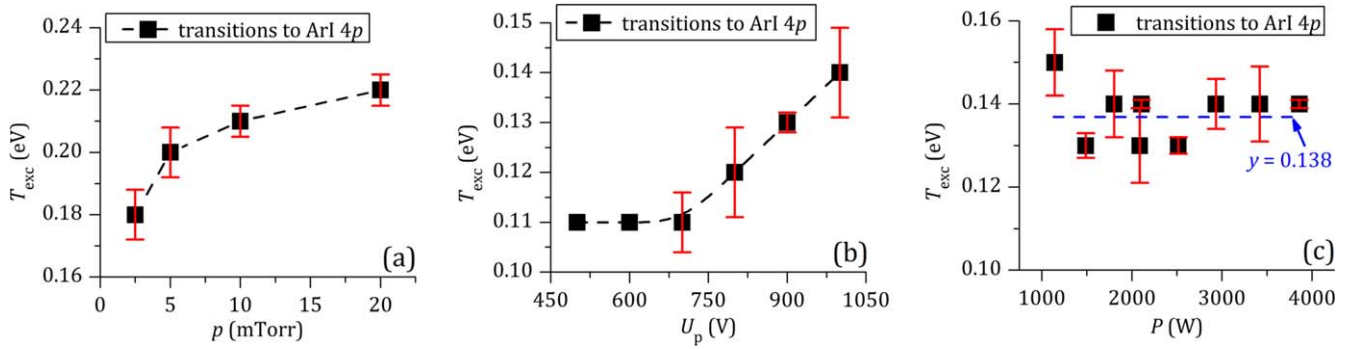


Figure 7. Electron excitation temperatures (T_{exc}) in the plasma near substrate as a function of pressure (p), pulse voltage (U_p), and discharge power (P).

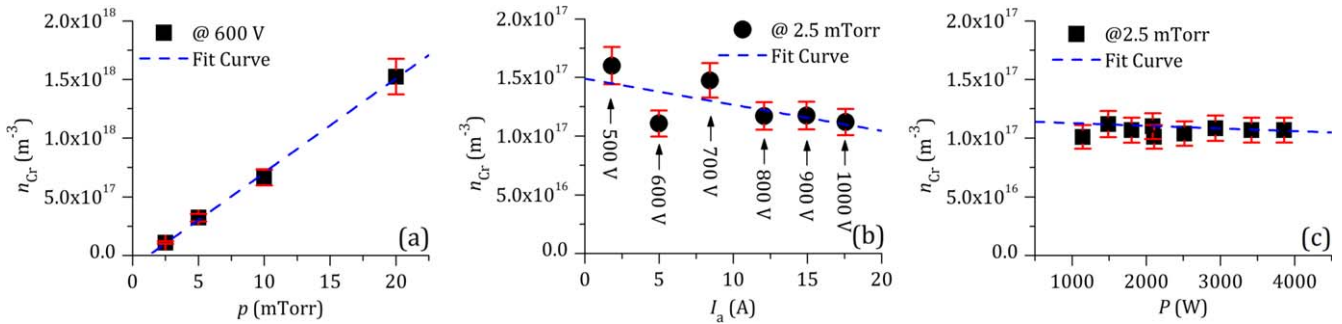


Figure 8. Dependence of the Cr density (n_{Cr}) in the near substrate region against the pressure (p), the average current (I_a) corresponding to the pulse voltage (U_p) and the discharge power (P).

Figure 7 shows the modified Boltzmann plot for the electron excitation temperatures. The energy, spontaneous emission probability, and statistical weights used for the calculations can be found in table 2. The electron excitation temperature increases with the pressure and the pulse voltage, but keeps nearly constant with the discharge power increasing from 1000 to 3000 W. The argon atoms are impacted by electrons and become excited and ionized. The extent of the Ar excitation depends on the energy of the electrons. The variation of emission line intensities for Ar and Cr neutrals we observed (in figures 3–5) is consistent with the change of the calculated electron temperature.

4.3. Determination of the neutral chromium atom density

As the generation of excited Ar atoms is a two-steps process (table 2), we calculated chromium neutral densities from the line intensities and the model described in section 2, equation (11). The emission of Cr line at 521.0 nm ($z^5P^o \rightarrow a^5S$) is selected and the Ar line at 605.5 nm ($3s^23p^55d \rightarrow 3s^23p^54p$) is used. The measured spectral response of the used 1200 g mm⁻¹ gratings with the 300 nm blaze for the two lines is about 0.80 and 0.68, respectively. Figure 8 shows the dependence of the Cr density on the pressure, average current (corresponding to the pulse voltage) and discharge power. We observe that the [Cr] increases linearly with the pressure. Assuming that the sputter yield is determined by the discharge voltage (no collisions for ions within the sheath), as the pulse voltage keeps constant for different pressures, the sputter rate is mainly influenced by the

ion density which would increase with the pressure. The results obtained with the increase of the average current were surprising. The sputter yield should increase with the pulse voltage, however no obvious increase of the [Cr] was observed. The present results can be understood on the basis of the thermalization of Cr sputtered atom. It is well known that in magnetron discharges the gas density is lower due to sputtered atoms which are ejected from the cathode with relatively high kinetic energy of several electron volts. This result is also accordance with the increase of electron temperature in figure 7(b).

The measured electron density under different pressure and pulse voltage conditions are given in figure 9. The measured electron density is in the orders of 10^{16} – 10^{17} m⁻³, which is at a comparable range performed by Vetushka *et al* [43]. The electron temperature obtained at the substrate vicinity through the Langmuir probe measuring varied in a range of 0.5–0.75 eV. These combined results would allow us to make conclusion on influence of the power on the ion to neutral ratio arriving to the substrate. As the plasma density goes up, the neutral density will goes down with the increase of the power in this experimental ranges.

5. Conclusions

We studied the emission spectra of near-substrate Cr HiPIMS plasma working in low density discharge mode under the conditions of gas pressure in the range of 2.5–20 mTorr, pulse voltage in the range of 400–1000 V, and discharge power less

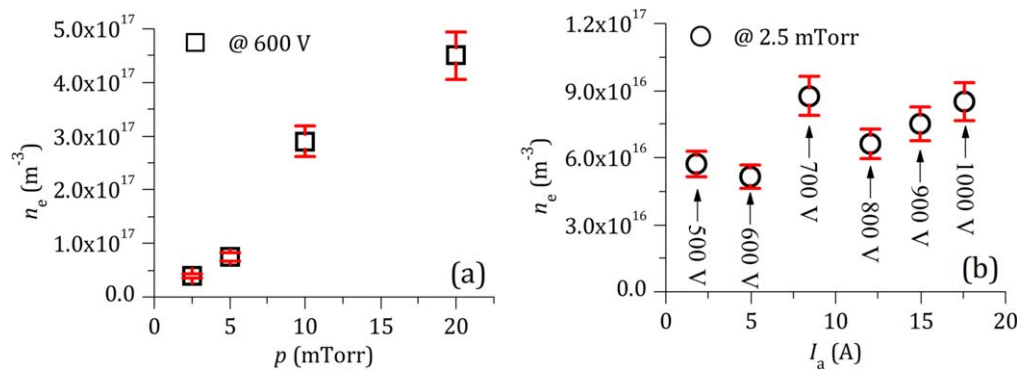


Figure 9. Dependence of the electron density (n_e) in the near substrate region against the pressure (p) and the average current (I_a) corresponding to the pulse voltage (U_p).

than 4000 W. The OES results showed that the Cr HiPIMS plasma was far from the LTE state, the loss mechanism of the activated species of the Cr HiPIMS plasma in the near-substrate region was a diffusion dominant process. A method to obtain the electron temperature based on corona balance of Ar excited atoms, combined with the predictions of a collisional-radiative model for neutral chromium atom density in Cr HiPIMS discharge has been presented. The number density of Cr neutral atoms was found to mainly be determined by the working pressure, and decrease with the increase of the pulse voltage and discharge power. The 10^{17} – 10^{18} m^{-3} chromium atom density indicates neutral atoms still count for the majority of the deposition species although the ion flux has been improved by HiPIMS compared with dcMS. These findings could lead to a better understanding of low density discharge HiPIMS plasma processes that maximize the activation of sputtered atoms, which provide valuable insights for the optimization of HiPIMS process to obtain the desired thin film properties.

Acknowledgments

This work was supported by the National Natural Science Foundation of China (11705258), National Science and Technology Major Project (2017-VII-0012-0108), Ningbo Science and Technology Innovation Project (2018B10014).

ORCID iDs

Xiao Zuo  <https://orcid.org/0000-0002-3215-208X>
 Aiying Wang  <https://orcid.org/0000-0003-2938-5437>

References

- [1] Gudmundsson J T 2010 The high power impulse magnetron sputtering discharge as an ionized physical vapor deposition tool *Vacuum* **84** 1360
- [2] Gudmundsson J T, Brenning N, Lundin D and Helmersson U 2012 High power impulse magnetron sputtering discharge *J. Vac. Sci. Technol. A* **30** 030801
- [3] Ehiasarian A P, Vetushka A, Hecimovic A and Konstantinidis S 2008 Ion composition produced by high power impulse magnetron sputtering discharges near the substrate *J. Appl. Phys.* **104** 083305
- [4] Hecimovic A and Ehiasarian A P 2010 Spatial and temporal evolution of ion energies in high power impulse magnetron sputtering plasma discharge *J. Appl. Phys.* **108** 063301
- [5] Kozak T, Vlcek J and Kos S 2013 Transport and ionization of sputtered atoms in high-power impulse magnetron sputtering discharges *J. Phys. D: Appl. Phys.* **46** 105203
- [6] Ehiasarian A P, Vetushka A, Gonzalvo Y A, Safran G, Szekely L and Barna P B 2011 Influence of high power impulse magnetron sputtering plasma ionization on the microstructure of TiN thin films *J. Appl. Phys.* **109** 104314
- [7] Tiron V, Velicu I L, Cristea D, Lupu N, Stoian G and Munteanu D 2018 Influence of ion-to-neutral flux ratio on the mechanical and tribological properties of TiN coatings deposited by HiPIMS *Surf. Coat. Technol.* **352** 690
- [8] Reinhard C, Ehiasarian A P and Hovsepian P E 2007 Oxidation behaviour of nanoscale multilayer CrAlYN/CrN coatings deposited by the combined high power impulse magnetron sputtering/unbalanced magnetron sputtering technique *Plasma Process. Polym.* **4** S910
- [9] Bathgate S N, Ganesan R, Bilek M M M and McKenzie D R 2016 A HiPIMS plasma source with a magnetic nozzle that accelerates ions: application in a thruster *Eur. Phys. J.-Appl. Phys.* **76** 30801
- [10] Azuma K and Kimura T 2016 Plasma parameters of titanium-based metallic plasma generated by a compact-type high-power pulsed sputtering penning discharge *IEEE Trans. Plasma Sci.* **44** 3201
- [11] Andersson J and Anders A 2009 Self-sputtering far above the runaway threshold: an extraordinary metal-ion generator *Phys. Rev. Lett.* **102** 045003
- [12] Cemin F, Lundin D, Cammilleri D, Maroutian T, Lecoer P and Minea T 2016 Low electrical resistivity in thin and ultrathin copper layers grown by high power impulse magnetron sputtering *J. Vac. Sci. Technol. A* **34** 051506
- [13] Stranak V, Kratochvil J, Olejnicek J, Ksirova P, Sezemsky P, Cada M and Hubicka Z 2017 Enhanced oxidation of TiO₂ films prepared by high power impulse magnetron sputtering running in metallic mode *J. Appl. Phys.* **121** 171914
- [14] Han X C, Xue J X, Peng S M and Zhang H B 2019 An interesting oxidation phenomenon of Cr coatings on Zry-4 substrates in high temperature steam environment *Corros. Sci.* **156** 117
- [15] Wu A, Ribis J, Brachet J C, Clouet E, Lepretre F, Bordas E and Arnal B 2018 HRTEM and chemical study of an ion-irradiated chromium/zircaloy-4 interface *J. Nucl. Mater.* **504** 289

- [16] Brenning N and Lundin D 2012 Alfvén's critical ionization velocity observed in high power impulse magnetron sputtering discharges *Phys. Plasmas* **19** 093505
- [17] Brenning N, Lundin D, Minea T, Costin C and Vitelaru C 2013 Spokes and charged particle transport in HiPIMS magnetrons *J. Phys. D: Appl. Phys.* **46** 084005
- [18] Ehiasarian A P, Hecimovic A, de los Arcos T, New R, Schulz-von der Gathen V, Boke M and Winter J 2012 High power impulse magnetron sputtering discharges: instabilities and plasma self-organization *Appl. Phys. Lett.* **100** 114101
- [19] Gudmundsson J T, Lundin D, Stancu G D, Brenning N and Minea T M 2015 Are the argon metastables important in high power impulse magnetron sputtering discharges? *Phys. Plasmas* **22** 113508
- [20] Sarakinos K, Alami J and Konstantinidis S 2010 High power pulsed magnetron sputtering: a review on scientific and engineering state of the art *Surf. Coat. Technol.* **204** 1661
- [21] Anders A, Capek J, Hala M and Martinu L 2012 The 'recycling trap': a generalized explanation of discharge runaway in high-power impulse magnetron sputtering *J. Phys. D: Appl. Phys.* **45** 012003
- [22] Wiatrowski A, Posadowski W M and Radzimski Z J 2008 Pulsed dc self-sustained magnetron sputtering *J. Vac. Sci. Technol. A* **26** 1277
- [23] Anders A 2008 Self-sputtering runaway in high power impulse magnetron sputtering: the role of secondary electrons and multiply charged metal ions *Appl. Phys. Lett.* **92** 201501
- [24] Ehiasarian A P, New R, Munz W D, Hultman L, Helmersson U and Kouznetsov V 2002 Influence of high power densities on the composition of pulsed magnetron plasmas *Vacuum* **65** 147
- [25] Hala M, Viau N, Zabeida O, Klemberg-Sapieha J E and Martinu L 2010 Dynamics of reactive high-power impulse magnetron sputtering discharge studied by time- and space-resolved optical emission spectroscopy and fast imaging *J. Appl. Phys.* **107** 043305
- [26] Breilmann W, Maszl C, Hecimovic A and von Keudell A 2017 Influence of nitrogen admixture to argon on the ion energy distribution in reactive high power pulsed magnetron sputtering of chromium *J. Phys. D: Appl. Phys.* **50** 135203
- [27] Britun N, Minea T, Konstantinidis S and Snyders R 2014 Plasma diagnostics for understanding the plasma-surface interaction in HiPIMS discharges: a review *J. Phys. D: Appl. Phys.* **47** 224001
- [28] Ryan P J, Bradley J W and Bowden M D 2019 Comparison of Langmuir probe and laser Thomson scattering for electron property measurements in magnetron discharges *Phys. Plasmas* **26** 073515
- [29] Ryan P J, Bradley J W and Bowden M D 2019 Comparison of Langmuir probe and laser Thomson scattering for plasma density and electron temperature measurements in HiPIMS plasma *Phys. Plasmas* **26** 040702
- [30] Zuo X, Ke P L, Chen R D, Li X W, Oden M and Wang A Y 2017 Discharge state transition and cathode fall thickness evolution during chromium HiPIMS discharge *Phys. Plasmas* **24** 083507
- [31] Wendt A E and Lieberman M A 1990 Spatial structure of a planar magnetron discharge *J. Vac. Sci. Technol. A* **8** 902
- [32] Guimaraes F and Bretagne J 1993 Study of an argon magnetron discharge used for molybdenum sputtering: I. Collisional radiative model *Plasma Sources Sci. Technol.* **2** 127
- [33] Zambrano G, Riascos H, Prieto P, Restrepo E, Devia A and Rincon C 2003 Optical emission spectroscopy study of r.f. magnetron sputtering discharge used for multilayers thin film deposition *Surf. Coat. Technol.* **172** 144
- [34] Weiss Z 2019 Excitation and ionization of iron in argon and neon glow discharges: towards the true picture *Spectrochim. Acta B* **158** 105637
- [35] Vandersijde B and Vandermullen J A M 1990 Temperature determination in non-LTE plasmas *J. Quant. Spectrosc. Radiat.* **44** 39
- [36] Song M A, Lee Y W and Chung T H 2011 Characterization of an inductively coupled nitrogen-argon plasma by Langmuir probe combined with optical emission spectroscopy *Phys. Plasmas* **18** 023504
- [37] Kramida A, Ralchenko Y, Reader J and NIST ASD Team 2018 *NIST Atomic Spectra Database (ver. 5.6.1)* (Gaithersburg MD: National Institute of Standards and Technology) <https://physics.nist.gov/asd>
- [38] Vitelaru C, Lundin D, Stancu G D, Brenning N, Bretagne J and Minea T 2012 Argon metastables in HiPIMS: time-resolved tunable diode-laser diagnostics *Plasma Sources Sci. Technol.* **21** 025010
- [39] Stancu G D, Brenning N, Vitelaru C, Lundin D and Minea T 2015 Argon metastables in HiPIMS: validation of the ionization region model by direct comparison to time resolved tunable diode-laser diagnostics *Plasma Sources Sci. Technol.* **24** 045011
- [40] Kanitz A, Hecimovic A, Boke M and Winter J 2016 Two dimensional spatial Argon metastable dynamics in HiPIMS discharges *J. Phys. D: Appl. Phys.* **49** 125203
- [41] Nouvellon C, Konstantinidis S, Dauchot J P, Wautelet M, Jouan P Y, Ricard A and Hecq M 2002 Emission spectrometry diagnostic of sputtered titanium in magnetron amplified discharges *J. Appl. Phys.* **92** 32
- [42] Gaillard M, Britun N, Kim Y M and Han J G 2007 Titanium density analysed by optical absorption and emission spectroscopy in a dc magnetron discharge *J. Phys. D: Appl. Phys.* **40** 809
- [43] Vetushka A and Ehiasarian A P 2007 Plasma dynamic in chromium and titanium HiPIMS discharges *J. Phys. D: Appl. Phys.* **41** 015204